SPECT Study of Folate Receptor-Positive Malignant and Normal Tissues in Mice Using a Novel ^{99m}Tc-Radiofolate

Cristina Müller[1], Flavio Forrer[1], Roger Schibli[2,3], Eric P. Krenning[1], and Marion de Jong[1]

[1]Department of Nuclear Medicine, Erasmus Medical Center, Rotterdam, The Netherlands; [2]Center for Radiopharmaceutical Science, Paul Scherrer Institute, ETH-PSI-USZ, Villigen, Switzerland; and [3]Department of Chemistry and Applied Biosciences, ETH Zurich, Zurich, Switzerland

The folate receptor (FR) is overexpressed on epithelial cancers (FR-α) and on activated, but not resting, macrophages (FR-β) involved in a variety of inflammatory and autoimmune diseases. Therefore, folate-based radiopharmaceuticals have the potential to be used as imaging agents of FR-positive tumor and inflammatory cells. In this study SPECT/CT of FR-positive malignant and normal tissues and organs in mice was performed using an improved organometallic ^{99m}Tc-radiofolate. **Methods:** The ^{99m}Tc radiolabeling of the histidine-folate was performed using the tricarbonyl technique described earlier for preparation of other organometallic radiofolates. Nude male mice with FR-positive KB tumor xenografts were used. Biodistribution studies were performed 1, 4, and 24 h after injection of the ^{99m}Tc-His-folate (1.5 MBq/mouse). Images were acquired with a dedicated small-animal SPECT/CT camera 24 h after injection of the radiofolate (500 MBq/mouse). Ex vivo autoradiography was performed on tumors and FR-positive normal tissues. Adjacent sections were used for in vitro autoradiography of FRs after decay of the injected radioactivity. **Results:** The SPECT/CT studies revealed accumulation of the radiotracer in FR-positive KB tumor xenografts and kidneys as reported previously. At the same time, specific uptake of the radiofolate in normal tissues—that is, salivary glands and choroid plexus—could be visualized with SPECT. FR-specific accumulation in these tissues and organs was confirmed by coinjection of excess folic acid, which resulted in a complete blockade of radiofolate uptake. In addition, ex vivo and in vitro autoradiography of these organs and tissues confirmed FR expression and displayed radioactivity distribution patterns almost identical to those found on SPECT images. In biodistribution studies we found a high tumor uptake (4.29 ± 0.67 %ID/g [percentage of the injected dose per gram of tissue], 4 h after injection) that was almost completely retained over time (3.51 ± 0.37 %ID/g, 24 h after injection). **Conclusion:** The novel ^{99m}Tc-histidine-folate showed improved in vivo characteristics compared with other organometallic radiofolates that allowed imaging of FR-positive malignant (KB tumor xenografts) and kidneys. For the first time, to our knowledge, specific tracer uptake in salivary glands and the choroid plexus could be visualized using a high-resolution animal SPECT/CT camera.

Key Words: folate receptor; choroid plexus; salivary glands; histidine-folate; SPECT/CT

J Nucl Med 2008; 49:310–317
DOI: 10.2967/jnumed.107.045856

The folate receptor (FR) is overexpressed on epithelial cancers (FR-α) (e.g., ovarian, endometrial carcinomas) (*1*) and on activated, but not resting, macrophages (FR-β) involved in a variety of inflammatory and autoimmune diseases (e.g., rheumatoid arthritis) (*2,3*). Interest has been sparked in using folic acid as a molecular "Trojan horse" to deliver diagnostic or therapeutic probes attached to the vitamin specifically into FR-positive tumor or inflammatory cells (*4–6*).

In the last decade, several attempts were undertaken to develop folate-based radiopharmaceuticals for imaging of FR-positive malignant tissue and inflammation (*7*). A variety of diagnostic radionuclides has been investigated for folate-based SPECT and PET (e.g., ^{99m}Tc (*8–10*), ^{111}In (*11*), ^{66,67,68}Ga (*12,13*), ^{18}F (*14*)). ^{99m}Tc is the preferred diagnostic radionuclide because of favorable decay properties (6-h half-life; γ-radiation of 140 keV) that allow administration of large doses, to yield high-resolution images, as well as low cost and easy on-site availability by the ^{99}Mo/^{99m}Tc-generator in the clinic.

As for any tumor-related structure to be targeted, the question arises whether these receptors are expressed in normal tissues and organs, because this could result in undesired accumulation of the targeting agent in healthy tissue. Several studies have been performed to answer this question for FRs (*15–17*). In normal organs and tissues, significant levels of FRs are expressed in some epithelia involved in retention and uptake/reabsorption of folates, which act as cofactors of enzymes involved in the biosynthesis of nucleotide bases and the amino acid metabolism. These are primarily the kidneys, the placenta, and the choroid plexus. FRs have been reported to be localized to the apical

Received Aug. 1, 2007; revision accepted Nov. 7, 2007.
For correspondence or reprints contact: Cristina Müller, PhD, Department of Nuclear Medicine, Erasmus Medical Center, s-Gravendijkwal 230, 3015 CE Rotterdam, The Netherlands.
E-mail: cristina.mueller@psi.ch

surfaces of polarized epithelia and, thus, inaccessible to folate conjugates in the blood (*16–19*). However, as shown in biodistribution studies, FR expression on the renal brush-border membrane (*20,21*) leads to high radioactivity accumulation in the kidneys as a result of reabsorption of radiofolates from primary urine (*8,9,11,22*). Beside kidneys, placenta, and choroid plexus, FRs have been identified in salivary glands. Holm et al. stated that the folate-binding protein (soluble form of the FR) present in the saliva from humans is a secretory product thereof (*23*).

Although many tumor-targeting studies with folate-based radiopharmaceuticals have been reported in the literature, little attention has been concentrated on undesired FR targeting in healthy tissues and organs. Because preclinical studies of radiopharmaceuticals were limited to biodistribution studies while investigating standard organs, the potential accumulation in FR-positive normal tissues, such as the choroid plexus or the salivary glands, has not been taken into consideration.

The aims of this study were to investigate the tissue distribution of the novel organometallic ^{99m}Tc-radiofolate (^{99m}Tc-His-folate) and to perform SPECT/CT studies on (FR-positive) KB tumor-bearing mice using a dedicated, high-resolution/high-sensitivity small-animal SPECT/CT camera. In addition, ex vivo and in vitro autoradiography studies were performed to investigate the distribution patterns and confirm specificity of the radiofolate in FR-positive malignant and normal tissues and organs of mice.

MATERIALS AND METHODS

Synthesis

The His-folate was synthesized in collaboration with Merck Eprova AG, Schaffhausen, Switzerland, and the Department of Chemistry and Biological Chemistry, University of Applied Sciences, Winterthur, Switzerland. The detailed description of the organic synthesis of the histidine-$(CH_2)_4$-γ-folate derivative (referred to as His-folate) will be described elsewhere. For the preparation of the chelating system that was coupled to folic acid via a spacer group, we applied the recently published synthetic strategy (*24,25*). In brief, the fully protected $^{\tau}$N-functionalized histidine-chelator was coupled to the γ-carboxylate group of doubly protected glutamic acid. After deprotection at the N-terminus of the glutamate moiety, it was coupled to the activated pteroic acid precursor. The fully protected folate intermediate was then deprotected to obtain the crude His-folate derivative that was purified by means of semipreparative high-performance liquid chromatography (HPLC). Scheme 1 of the synthetic strategy and the NMR analysis of the final product are available as supplemental material online only at http://jnm.snmjournals.org.

Radiofolate Synthesis

Pertechnetate ([Na][^{99m}TcO$_4$]) was eluted from a ^{99}Mo/^{99m}Tc-generator (Mallinckrodt-Tyco) with a 0.9% saline solution. The tricarbonyl precursor $[^{99m}Tc(OH_2)_3(CO)_3]^+$ was prepared using the IsoLink kit (Mallinckrodt-Tyco). The ^{99m}Tc-His-folate was prepared by addition of the tricarbonyl precursor (1.7 GBq, 450 μL) to a solution of the His-folate (2.5 nmol) in phosphate-buffered saline (PBS, pH 7.4; 50 μL), resulting in a specific activity of 680 MBq/nmol. The sealed reaction vial was heated for 60 min at 80°C (Fig. 1). Quality control was performed by HPLC (Waters) using a symmetry (Waters) C-18 reversed-phase column with an eluent system consisting of methanol and triethylammonium phosphate buffer (pH 7.0) with a gradient of 0%–90% methanol over 35 min (His-folate, R_t [retention time] = 16.3 min; ^{99m}Tc-His-folate, R_t = 19.5 min). The final radiochemical purity of the ^{99m}Tc-His-folate was >98% (determined by HPLC).

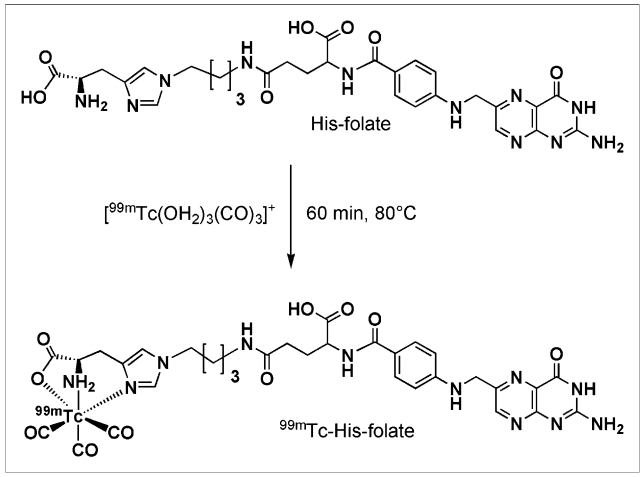

FIGURE 1. ^{99m}Tc radiolabeling of His-folate ligand using the tricarbonyl technique.

To achieve optimal imaging conditions for SPECT/CT studies, the injection of a high amount of radioactivity was necessary (~500 MBq, 1 nmol/mouse). However, for biodistribution studies, the ^{99m}Tc-His-folate tracer was separated from the unlabeled His-folate ligand by means of HPLC, giving rise to the highest specific activity achievable (*25*).

Cell Culture

KB cells (human nasopharyngeal carcinoma cell line) were purchased from the American Type Culture Collection (CCL-17). The cells were cultured as monolayers at 37°C in a humidified atmosphere containing 5% CO_2. Importantly, the cells were cultured in FFRPMI cell culture medium (modified RPMI medium, without folic acid, vitamin B_{12}, and phenol red; Cell Culture Technologies GmbH). FFRPMI medium was supplemented with 10% heat-inactivated fetal calf serum (as the only source of folate), L-glutamine, and antibiotics (penicillin/streptomycin/fungizone).

Biodistribution in Tumor-Bearing Mice

All animal experiments were approved by the governing Animal Welfare Committee and conducted in accordance with the regulations of the Erasmus Medical Center, Rotterdam. Eight- to 10-wk-old male, athymic nude mice (NMRI *nu/nu*) were purchased from Charles River Laboratories. The animals were acclimatized and fed a folate-deficient rodent diet starting 5 d before the tumor cell inoculation (*26*). The mice were inoculated subcutaneously with KB tumor cells (suspension of 5×10^6 cells in 100 μL PBS) on each shoulder. Radiofolate biodistribution studies were performed in triplicate 14 d after tumor cell inoculation, when the tumors reached a size of 0.5–1.5 cm^3. For biodistribution studies, mice were injected with 1.5 MBq of ^{99m}Tc-His-folate in 100 μL PBS, administered via a lateral tail vein. The animals were sacrificed at 1, 4, or 24 h after injection of ^{99m}Tc-His-folate. Blocking experiments were performed 4 h after injection, with

mice coinjected with excess folic acid (100 μg). Selected tissues and organs were removed and weighed, and radioactivity was counted in a γ-counter (Wizard 1480; Perkin Elmer). The results were expressed as percentage of the injected dose per gram of tissue (% D/g), using reference counts from a definite sample of the original injectate counted at the same time.

SPECT/CT

SPECT/CT was performed with a 4-head multiplexing multipinhole camera (NanoSPECT/CT; Bioscan Inc.) (*27*). Each head was outfitted with a tungsten-based collimator of nine 1.4-mm-diameter pinholes, imaging a cylindric field of view that is 37 mm in diameter by 16 mm in length. The axial field of view is extended using a step-and-shoot helical (SPECT) or continuous (CT) acquisition mode with the user defining a range of 16–230 mm according to the region to be imaged. The apertures used in this study provided a reconstructed resolution in the submillimeter range at 140 keV. The acquisitions were performed overnight after euthanasia of the animals, approximately 24 h after injection of the ^{99m}Tc-His-folate. The time per view was chosen for 1,000 s. CT scans were performed with the integrated CT using a tube voltage of 45 kV and an exposure time of 1,500 ms per view. After acquisition, SPECT data were reconstructed iteratively with HiSPECT software (Scivis GmbH). The CT reconstruction used a cone-beam filtered backprojection. SPECT and CT data were automatically coregistered as both modalities shared the same axis of rotation. The fused datasets were analyzed in the InVivoScope postprocessing software (Bioscan, Inc.).

Ex Vivo Autoradiography

For autoradiography studies, mice were injected with ^{99m}Tc-His-folate (~70 MBq) and sacrificed 4–5 h after injection. Immediately after euthanasia, tumors, kidneys, salivary glands, and the brain were collected and frozen, embedded in TissueTek (O.C.T. Compound; Sakura Finetek Europe B.V.), and stored at −80°C. Frozen tissues and organs were cut into 10-μm sections with a microtome (HM 560 M; Cryo-Star) and mounted on slides (Superfrost plus; Menzel). The slides were exposed to phosphor imaging screens (type SR, 12.5 × 25.2 cm^2; Packard Instruments Co.) in x-ray cassettes overnight. The screens were then read by a phosphor imager (Cyclone; Packard, Instruments Co.) to reveal distribution of radioactivity in the sections.

In Vitro Autoradiography

After decay of radioactivity, in vitro autoradiography of FRs was performed on sections adjacent to those prepared for ex vivo autoradiography, allowing comparison of FR expression and radioactivity distribution in the ex vivo sections. The slides with tissue sections were preincubated in Tris-HCl buffer (170 mM, pH 7.6, with 5 mM $MgCl_2$) with 0.25% (w/v) bovine serum albumin (BSA) for 10 min at room temperature. Then, the sections were incubated with a solution of ^{99m}Tc-His-folate (0.5 MBq/mL in Tris-HCl buffer containing 1% BSA) for 60 min at room temperature. After incubation, the sections were rinsed twice for 5 min in cold Tris-HCl buffer (with 25% BSA), then washed for 5 min in pure Tris-HCl buffer, and finally rinsed with cold distilled water. The sections were air-dried and exposed to phosphor imaging screens.

RESULTS

Radiolabeling

Radiolabeling of the His-folate was performed in 2 steps using the IsoLink method as described for preparation of other organometallic radiofolates (Fig. 1) (*22,24*). The labeling efficiency of the His-folate was significantly improved, allowing a half-maximal radiochemical yield at a lower ligand concentration (1.7×10^{-7} M) than necessary to radiolabel our previously described folate ligands (e.g., picolylamine monoacetic acid [PAMA]-folate; half-maximal yield at a ligand concentration of 1.6×10^{-6} M) (*28*). The higher specific activity achievable with this novel folate tracer made the separation of the radiofolate from unlabeled ligand obsolete for SPECT studies.

Biodistribution in Tumor-Bearing Mice

In vivo tissue distribution was investigated in male athymic nude mice, bearing KB tumor xenografts. The animals were sacrificed and dissected 1, 4, or 24 h after intravenous injection of the ^{99m}Tc-His-folate (Table 1). The tumor accumulation of radioactivity was high already at 1 h after injection (2.63 ± 0.48 %ID/g). The maximal tumor accumulation was found after 4 h (4.29 ± 0.67 %ID/g; $P < 0.001$) and was almost completely retained over the time of investigation (3.51 ± 0.37 %ID/g, 24 h after injection; $P = 0.037$). Clearance from the blood was fast, leading to increasing tumor-to-blood ratios of radioactivity over time (from 18.56 ± 10.47 at 1 h after injection to 184.23 ± 65.88 at 24 h after injection). Nonspecific retention of radioactivity in nontargeted organs and tissues (spleen, liver, muscle, bone) was low. Relatively high radioactivity, however, was found in the intestinal contents (~20 %ID/g at 1 h after injection, ~10 %ID/g at 4 h after injection, <1 %ID/g at 24 h after injection), indicating that the radiotracer was partially excreted via the gastrointestinal tract. Significant accumulation of radioactivity was found in the kidneys (24.56 ± 3.17 %ID/g; 4 h after injection) and salivary glands (5.72 ± 0.63 %ID/g, 4 h after injection). These values decreased rapidly over time (kidneys: 6.70 ± 1.12 %ID/g, salivary glands: 1.58 ± 0.69 %ID/g, 24 h after injection). Experiments with coinjected folic acid in excess showed an almost complete blockade in the tumor tissue (<0.1 %ID/g, 4 h after injection), the kidneys (<0.5 %ID/g, 4 h after injection), and the salivary glands (<0.01 %ID/g, 4 h after injection), indicating the FR-specific uptake of radiofolate in these tissues and organs.

SPECT/CT

SPECT/CT scans were performed with euthanized mice 24 h after injection of ~500 MBq of ^{99m}Tc-His-folate. At earlier time points (4 h after injection) the high radioactivity accumulation in the intestinal tract limited, in particular, the quality of whole-body scans. However, after 18–24 h, when the main abundance of radioactivity had cleared from nontargeted tissues, we were able to acquire high-quality whole-body scans (Fig. 2). High accumulation of radioactivity was detected in FR-positive KB tumors localized on both shoulders. The radiofolate could be localized basically only in the outer rim of the tumors. Significant accumulation of radioactivity was found in the kidneys, which was in

TABLE 1
Biodistribution Data of ^{99m}Tc-His-Folate in Athymic Nude Male Mice Bearing KB Tumor Xenografts

Tissue or ratio	%ID/g (mean ± SD)			
	1 h after injection	4 h after injection	24 h after injection	4 h after injection*
Blood	0.18 ± 0.10	0.12 ± 0.02	0.02 ± 0.01	<0.01
Heart	3.60 ± 0.53	1.16 ± 0.36	0.14 ± 0.07	<0.01
Lung	1.04 ± 0.12	0.69 ± 0.09	0.16 ± 0.07	<0.01
Spleen	0.37 ± 0.22	0.30 ± 0.04	0.05 ± 0.01	<0.01
Kidneys	23.96 ± 10.11	24.56 ± 3.17	6.70 ± 1.12	0.30 ± 0.31
Stomach	1.71 ± 0.12	1.03 ± 0.22	0.15 ± 0.02	0.02 ± 0.02
Intestines	3.84 ± 2.23	1.51 ± 0.29	0.18 ± 0.14	0.17 ± 0.06
Liver	9.73 ± 1.32	3.83 ± 1.49	0.44 ± 0.31	0.20 ± 0.03
Muscle	1.56 ± 0.07	1.09 ± 0.26	0.19 ± 0.03	<0.01
Bone	0.77 ± 0.07	0.58 ± 0.20	0.06 ± 0.01	<0.01
Salivary glands	6.52 ± 1.04	5.72 ± 0.63	1.58 ± 0.69	<0.01
Tumor	2.63 ± 0.48	4.29 ± 0.67	3.51 ± 0.37	0.06 ± 0.01
Tumor-to-blood	18.56 ± 10.47	38.00 ± 8.33	184.23 ± 65.88	
Tumor-to-liver	0.30 ± 0.06	1.19 ± 0.47	10.99 ± 5.60	
Tumor-to-kidney	0.12 ± 0.05	0.18 ± 0.03	0.53 ± 0.10	

*Coinjection of excess folic acid.
n = 3 mice.

accordance with our ex vivo biodistribution data. Activity was distributed in the cortex, where FRs are expressed. Diffuse radioactivity accumulation found in the region of the neck could be attributed to the tissue of the salivary glands (Fig. 3). Small designated areas in the brain showed high radioactivity accumulation and could be ascribed to the choroid plexus (Fig. 4).

Ex Vivo Autoradiography and In Vitro Autoradiography

Ex vivo and in vitro autoradiograms of the KB tumor and kidney sections are shown in Figure 5. Ex vivo autoradiograms of tumor sections showed that the radioactivity after injection accumulated primarily in the outer rim of the tumors, whereas nonradioactive areas were detected deeper in the tumor tissue (Fig. 5A). In contrast, when adjacent tumor sections were tested in vitro by adding ^{99m}Tc-Hisfolate after decay of the injected radioactivity, we found a homogeneous distribution of FR-bound radioactivity throughout the entire tumor tissue (Fig. 5B). Ex vivo autoradiograms of kidney sections showed a high accumulation of radioactivity in the cortex. This distribution pattern of bound radioactivity was also found on in vitro autoradiograms (Fig. 5). Kidneys and tumors of mice coinjected with excess folic acid showed almost complete blockade of radioactivity in the cortex, and only residual traces of radioactivity were found in the outer medulla (data not shown). Together, these findings clearly indicate the FR-specific accumulation of radioactivity in the renal cortex. Ex vivo autoradiograms from salivary glands proved the radioactivity accumulation distributed homogeneously throughout these

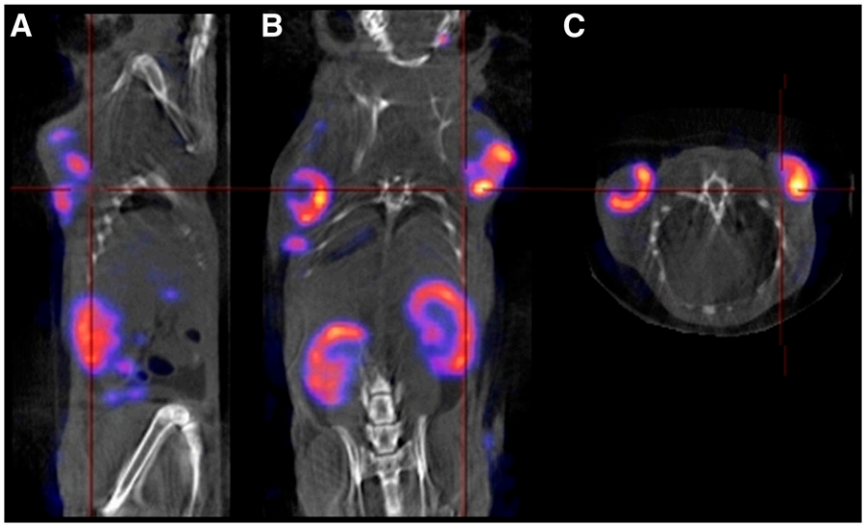

FIGURE 2. SPECT/CT images of a KB tumor-bearing mouse: sagittal (A), coronal (B), and transaxial (C) sections. Radiofolate accumulation is visible in KB tumor xenografts localized on both shoulders and in kidneys.

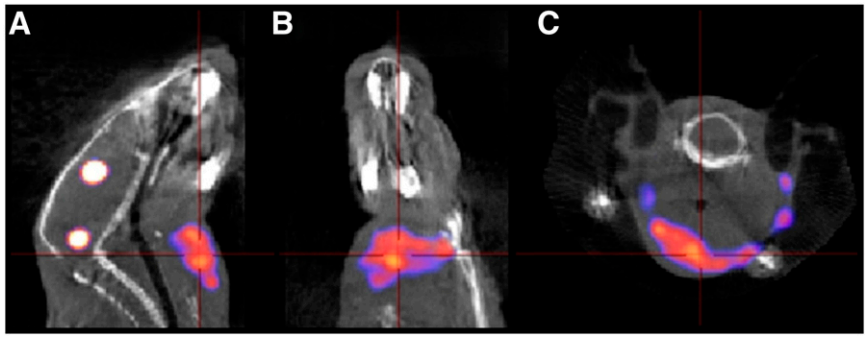

FIGURE 3. SPECT/CT images of salivary glands as sagittal (A), coronal (B), and transaxial (C) sections.

tissues and in vitro autoradiography proved again FR-specific uptake (data not shown).

Ex vivo brain sections of mice 4 h after injection of radioactivity revealed distinct areas with high tracer uptake. This uptake proved to be specific, as it was completely displaceable by coinjection of excess folic acid in vivo. In vitro autoradiograms of adjacent brain sections showed largely the same radioactivity accumulation pattern as that shown on ex vivo autoradiograms, and blocking experiments with folic acid showed a complete blockade of radiofolate binding (Fig. 6). The specific uptake could be attributed to the choroid plexus.

DISCUSSION

SPECT and PET offer unique capabilities for noninvasive probing of clinically relevant, tumor-associated molecular targets by means of selective and specific radiotracers. At the same time, the application of radiotracers enables the identification of tissue biochemistry and pathophysiology. The FR emerged as a promising tumor-associated target, and many endeavors have been undertaken for the development of folate-based diagnostic and therapeutic (radio)-pharmaceuticals (*6,7,29*). However, although FRs are restricted to a few sites in normal human tissues and organs (*15,16*), this could interfere with the detection of small FR-positive solid tumors and metastases on SPECT or PET images. In addition, normal FR-expressing cells risk damage by FR-targeted (radio)therapy.

The present study describes the FR-specific accumulation of a novel ^{99m}Tc-radiofolate in normal and malignant tissues and organs of KB tumor–xenografted mice. This became feasible because of the use of a dedicated small-animal SPECT/CT camera that allowed high spatial resolution and sensitivity and because of the application of a novel organometallic ^{99m}Tc-radiofolate. This radiotracer, ^{99m}Tc-His-folate, featured improved in vitro characteristics, allowing highly specific radiolabeling, and superior in vivo characteristics with a significantly higher tumor uptake than that of previously developed organometallic radiofolates (*22,24,25*).

Although SPECT and ex vivo autoradiography revealed accumulation of the radiotracer in the outer rim of the KB xenografts, in vitro autoradiography studies clearly confirmed a homogeneous expression of FRs throughout the entire tumor tissue and, thus, confirmed that the entire tumor volume was viable (Fig. 6B). Furthermore, determination of blood vessels with anti-CD31 antibodies against mouse blood vessels on sections of KB xenografts showed a relatively good vascularization. These in vivo and ex vivo observations suggest that a high intratumoral pressure in KB tumor xenografts was primarily the reason for the inhomogeneous tracer distribution.

High radioactivity retention in the cortex of the kidneys is a critical issue of the FR-targeting strategy in general. Because FRs are expressed on the luminal side of the brush-border membrane, they are exposed to the high folate-conjugate concentration present in the primary urine. As a consequence, (radio)folates significantly and specifically accumulate in the renal tissue. In particular, with regard to the development of therapeutic radiofolates, these findings are of concern.

Diffuse accumulation of radioactivity in the region of the neck prompted us to investigate whether this was the

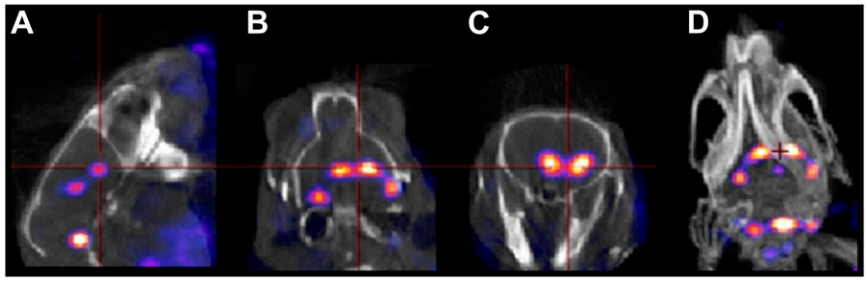

FIGURE 4. SPECT/CT images of mouse brain: choroid plexus as sagittal (A), coronal (B), and transaxial (C) section and in 3-dimensional planar view (D).

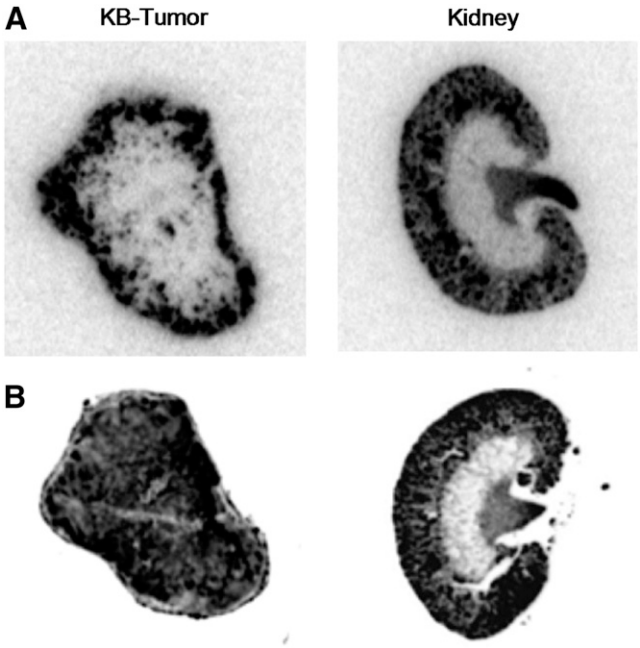

FIGURE 5. Ex vivo (A) and in vitro (B) autoradiograms of KB tumors and kidneys.

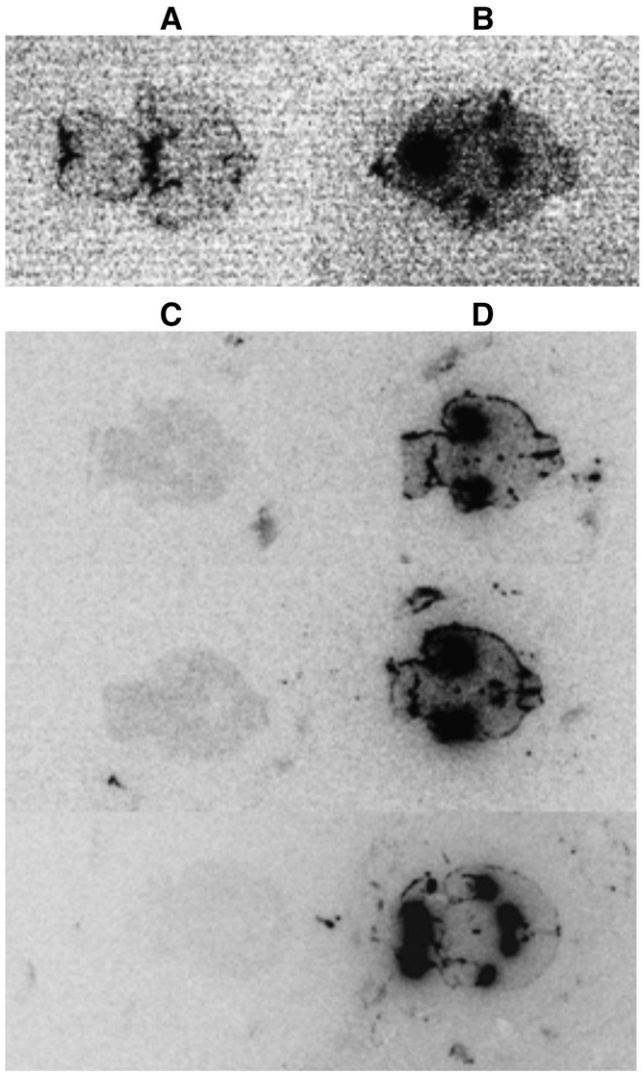

FIGURE 6. Ex vivo autoradiography: representative section of mouse brain after injection of ^{99m}Tc-radiofolate together with excess folic acid for FR blockade (A) or after injection of ^{99m}Tc-radiofolate only (B). In vitro autoradiography (performed after decay of injected radioactivity): sections of mouse brain at different levels incubated with ^{99m}Tc-radiofolate and excess folic acid for FR blockade (C) or ^{99m}Tc-radiofolate only (D).

consequence of a specific or nonspecific activity accumulation. Ex vivo and in vitro autoradiography studies performed with frozen sections of the salivary glands (sublingual glands and submaxillary glands) clearly confirmed the presence of FRs and the FR-specific accumulation of the ^{99m}Tc-radiotracer in these tissues, as excess cold folic acid was able to block radioactivity binding almost completely. Holm et al. reported the presence of the FR in human parotid glands and the folate-binding protein in human saliva (*23*). However, to date, there are no data on clinical trials in patients that report radiofolate accumulation in the salivary glands (*30*). Although no negative impact for radiofolate-based imaging is expected, it might be a critical issue again with regard to folate-based radiotherapy.

The choroid plexus, the anatomic locus of the blood–cerebrospinal fluid barrier, plays an important role in transport and homeostasis of vitamins and micronutrients in the central nervous system (*19*). Because folates were found at higher concentrations in the cerebrospinal fluid and brain of mammals compared with their concentrations in the plasma, they must enter the cerebrospinal fluid or brain from the blood and, consequently, a mechanism for the transfer might reside in the choroid plexus (*31*). Investigations by Holm et al. (*19*) and Weitman et al. (*16*) of human choroid plexus clearly indicated the presence of FRs in these tissues.

Kennedy et al. investigated the uptake of a radioactive folate conjugate, the ^{111}In-DTPA-folate (DTPA = diethylenetriaminepentaacetic acid), into the brain of BALB/c mice by quantitative determination of radioactivity in collected brain tissues after euthanasia (*32*). Repeated injections or prolonged release of the radiotracer via an osmotic pump did not result in an increased radioactivity uptake into the brain. Imaging studies of brain slices and whole brain tissue after injection of folate-fluorescein revealed fluorescence on all cells of the choroid plexus but virtually no fluorescence in other regions of the brain. From these results Kennedy et al. concluded that choroid plexus cells are able to concentrate small-molecular-weight folate conjugates from the blood but that there is no significant transport of the molecules across the blood–brain barrier. Our findings are in agreement with the results of Kennedy et al. We found radioactivity at small designated areas of the brain referred to as cells of the choroid plexus but no diffusion or transport within other regions of brain tissue. Kennedy et al. favor the conclusion that the FRs in the choroid plexus are inactive in transcytosing folic acid

conjugates into the brain. Although this conclusion could explain our findings, it seems to be in contradiction with Spector and Lorenzo, who reported the transport of folates via choroid plexus into the brain (*31*). However, it must be taken into consideration that Spector and Lorenzo investigated the fate of physiologic (reduced) folates such as 5-methyl tetrahydrofolate (5-Me-THF), which is likely to be different than that of folic acid and conjugates thereof. Folic acid, the oxidized form of folates, features increased FR-binding affinity compared with reduced folates, and distinct conditions are necessary for intracellular release (*33*).

What could be the consequences of our findings and which opportunities do we have to cope with potential side effects? High binding and uptake of radioactivity into the renal tissue is a logical consequence of FR expression in the proximal tubule cells, which is particularly undesirable with regard to the development of therapeutic radiofolates. However, recently a protocol was developed that describes the combined application of an antifolate (pemetrexed, Alimta; Eli Lilly & Co. (*34*)) and an organometallic ^{99m}Tc-radiofolate that resulted in a significant and selective decrease of radioactivity retention in the kidneys without affecting the tumor uptake in mice (*35*). Data obtained with ^{99m}Tc-His-folate used in this study and other radiofolates (e.g., ^{111}In-DTPA-folate) suggest that the protocol is applicable and effective with any radiofolate independent of the structure, the radionuclide, and chelating systems used. This would suggest the hypothesis that kidneys could also be protected from particle-emitting radiofolates designed for therapeutic purposes when mice are preinjected with pemetrexed. However, up to now, it remains unclear whether the "Alimta effect" holds true also in patients.

High and specific uptake of radioactivity could cause salivary hypofunction as a side effect of a folate-based radiotherapy. The cytoprotective agent amifostine (*36*)—approved by the Food and Drug Administration to anticipate radiation- and chemotherapy-induced kidney damage and hypofunction of salivary glands—is successfully applied in the clinics (*37*), and data from our group also showed the beneficial effect of amifostine for renal protection during peptide receptor radionuclide therapy in rats (*38*). Therefore, it is believed that amifostine could be used in combination with folate-based radiotherapy to protect both radiation-sensitive kidneys and salivary glands.

Undesired high and specific uptake of folate-based drugs in the choroid plexus could be detrimental. On the other hand, it could also provide opportunities for treatment of tumors of the choroid plexus. In fact, Patrick et al. investigated the distribution pattern of FRs in normal choroid plexus and choroid plexus tumors of simian virus 40 transgenic mice (*39*). Our preliminary data using a novel ^{111}In-labeled folate derivative seem to confirm these findings made with the organometallic ^{99m}Tc-His-folate. However, to the best of our knowledge, there are no reports on radiofolate (e.g., ^{111}In-DTPA-folate) uptake in the choroid plexus in humans.

CONCLUSION

In this study, we were able to image FR-positive malignant and normal tissues and organs in tumor-bearing mice using a newly developed high-affinity ^{99m}Tc-radiofolate and a dedicated small-animal SPECT/CT camera. The high resolution and sensitivity of the images allowed determination of the radioactivity distribution throughout the tumor tissue as well as the detection of radioactivity in the renal cortex, the salivary glands, and the choroid plexus. It will be interesting and important to verify whether radiofolates accumulate in the human choroid plexus as well—particularly, with regard to a potential therapeutic application of radiofolates.

ACKNOWLEDGMENTS

We thank Dr. Christian Lackas and Dr. Nils Schramm (Bioscan Inc.) for support with the NanoSPECT/CT. This project was financially supported by Mallinckrodt Tyco (The Netherlands) and Merck Eprova AG (Switzerland).

REFERENCES

1. Antony AC. Folate receptors. *Annu Rev Nutr.* 1996;16:501–521.
2. Paulos CM, Turk MJ, Breur GJ, Low PS. Folate receptor-mediated targeting of therapeutic and imaging agents to activated macrophages in rheumatoid arthritis. *Adv Drug Deliv Rev.* 2004;56:1205–1217.
3. Turk MJ, Breur GJ, Widmer WR, et al. Folate-targeted imaging of activated macrophages in rats with adjuvant-induced arthritis. *Arthritis Rheum.* 2002;46: 1947–1955.
4. Salazar MD, Ratnam M. The folate receptor: What does it promise in tissue-targeted therapeutics? *Cancer Metastasis Rev.* 2007;26:141–152.
5. Hilgenbrink AR, Low PS. Folate receptor-mediated drug targeting: from therapeutics to diagnostics. *J Pharm Sci.* 2005;94:2135–2146.
6. Leamon CP, Low PS. Folate-mediated targeting: from diagnostics to drug and gene delivery. *Drug Discov Today.* 2001;6:44–51.
7. Ke CY, Mathias CJ, Green MA. Folate-receptor-targeted radionuclide imaging agents. *Adv Drug Deliv Rev.* 2004;56:1143–1160.
8. Reddy JA, Xu LC, Parker N, Vetzel M, Leamon CP. Preclinical evaluation of ^{99m}Tc-EC20 for imaging folate receptor-positive tumors. *J Nucl Med.* 2004;45: 857–866.
9. Mathias CJ, Hubers D, Low PS, Green MA. Synthesis of [^{99m}Tc]DTPA-folate and its evaluation as a folate-receptor-targeted radiopharmaceutical. *Bioconjug Chem.* 2000;11:253–257.
10. Guo W, Hinkle GH, Lee RJ. ^{99m}Tc-HYNIC-folate: a novel receptor-based targeted radiopharmaceutical for tumor imaging. *J Nucl Med.* 1999;40:1563–1569.
11. Wang S, Luo J, Lantrip DA, et al. Design and synthesis of [^{111}In]DTPA-folate for use as a tumor-targeted radiopharmaceutical. *Bioconjug Chem.* 1997;8:673–679.
12. Mathias CJ, Wang S, Low PS, Waters DJ, Green MA. Receptor-mediated targeting of ^{67}Ga-deferoxamine-folate to folate-receptor-positive human KB tumor xenografts. *Nucl Med Biol.* 1999;26:23–25.
13. Mathias CJ, Lewis MR, Reichert DE, et al. Preparation of ^{66}Ga- and ^{68}Ga-labeled Ga(III)-deferoxamine-folate as potential folate-receptor-targeted PET radiopharmaceuticals. *Nucl Med Biol.* 2003;30:725–731.
14. Bettio A, Honer M, Müller C, et al. Synthesis and preclinical evaluation of a folic acid derivative labeled with ^{18}F for PET imaging of folate receptor-positive tumors. *J Nucl Med.* 2006;47:1153–1160.
15. Parker N, Turk MJ, Westrick E, Lewis JD, Low PS, Leamon CP. Folate receptor expression in carcinomas and normal tissues determined by a quantitative radioligand binding assay. *Anal Biochem.* 2005;338:284–293.
16. Weitman SD, Lark RH, Coney LR, et al. Distribution of the folate receptor GP38 in normal and malignant cell lines and tissues. *Cancer Res.* 1992;52:3396–3401.
17. Weitman SD, Weinberg AG, Coney LR, Zurawski VR, Jennings DS, Kamen BA. Cellular localization of the folate receptor: potential role in drug toxicity and folate homeostasis. *Cancer Res.* 1992;52:6708–6711.

18. Mantovani LT, Miotti S, Menard S, et al. Folate binding protein distribution in normal tissues and biological fluids from ovarian carcinoma patients as detected by the monoclonal antibodies MOv18 and MOv19. *Eur J Cancer.* 1994;30A: 363–369.
19. Holm J, Hansen SI, Hoiermadsen M, Bostad L. High-affinity folate binding in human choroid-plexus: characterization of radioligand binding, immunoreactivity, molecular heterogeneity and hydrophobic domain of the binding protein. *Biochem J.* 1991;280:267–271.
20. McMartin KE, Morshed KM, Hazenmartin DJ, Sens DA. Folate transport and binding by cultured human proximal tubule cells. *Am J Physiol.* 1992;263:F841–F848.
21. Sandoval RM, Kennedy MD, Low PS, Molitoris BA. Uptake and trafficking of fluorescent conjugates of folic acid in intact kidney determined using intravital two-photon microscopy. *Am J Physiol Cell Physiol.* 2004;287:C517–C526.
22. Müller C, Hohn A, Schubiger PA, Schibli R. Preclinical evaluation of novel organometallic ^{99m}Tc-folate and ^{99m}Tc-pteroate radiotracers for folate receptor-positive tumour targeting. *Eur J Nucl Med Mol Imaging.* 2006;33:1007–1016.
23. Holm J, Hansen SI, Hoier-Madsen M, Nichols CW. Characterization of a folate receptor in parotid gland and folate binding protein in saliva from humans: epitope relatedness to human milk folate binding protein. *APMIS.* 2000;108: 517–524.
24. Müller C, Dumas C, Hoffmann U, Schubiger PA, Schibli R. Organometallic ^{99m}Tc-technetium(I)- and Re-rhenium(I)-folate derivatives for potential use in nuclear medicine. *J Organomet Chem.* 2004;689:4712–4721.
25. Müller C, Schubiger PA, Schibli R. Synthesis and in vitro/in vivo evaluation of novel ^{99m}Tc$(CO)_3$-folates. *Bioconjug Chem.* 2006;17:797–806.
26. Mathias CJ, Wang S, Lee RJ, Waters DJ, Low PS, Green MA. Tumor-selective radiopharmaceutical targeting via receptor-mediated endocytosis of gallium-67-deferoxamine-folate. *J Nucl Med.* 1996;37:1003–1008.
27. Forrer F, Valkema R, Bernard B, et al. In vivo radionuclide uptake quantification using a multi-pinhole SPECT system to predict renal function in small animals. *Eur J Nucl Med Mol Imaging.* 2006;33:1214–1217.
28. Müller C, Schubiger PA, Schibli R. Isostructural folate conjugates radiolabeled with the matched pair ^{99m}Tc/^{188}Re: a potential strategy for diagnosis and therapy of folate receptor positive tumors. *Nucl Med Biol.* 2007;34:595–601.
29. Leamon CP, Reddy JA. Folate-targeted chemotherapy. *Adv Drug Deliv Rev.* 2004;56:1127–1141.
30. Siegel BA, Dehdashti F, Mutch DG, et al. Evaluation of ^{111}In-DTPA-folate as a receptor-targeted diagnostic agent for ovarian cancer: initial clinical results. *J Nucl Med.* 2003;44:700–707.
31. Spector R, Lorenzo AV. Folate transport by the choroid plexus in vitro. *Science.* 1975;187:540–542.
32. Kennedy MD, Jallad KN, Lu J, Low PS, Ben-Amotz D. Evaluation of folate conjugate uptake and transport by the choroid plexus of mice. *Pharm Res.* 2003;20:714–719.
33. Kamen BA, Smith AK. A review of folate receptor alpha cycling and 5-methyltetrahydrofolate accumulation with an emphasis on cell models in vitro. *Adv Drug Deliv Rev.* 2004;56:1085–1097.
34. Rollins KD, Lindley C. Pemetrexed: a multitargeted antifolate. *Clin Ther.* 2005;27:1343–1382.
35. Müller C, Brühlmeier M, Schubiger AP, Schibli R. Effects of antifolate drugs on the cellular uptake of radiofolates in vitro and in vivo. *J Nucl Med.* 2006;47:2057–2064.
36. van der Vijgh WJ, Peters GJ. Protection of normal tissues from the cytotoxic effects of chemotherapy and radiation by amifostine (Ethyol): preclinical aspects. *Semin Oncol.* 1994;21:2–7.
37. Shiboski CH, Hodgson TA, Ship JA, Schiodt M. Management of salivary hypofunction during and after radiotherapy. *Oral Surg Oral Med Oral Pathol Oral Radiol Endod.* 2007;103(suppl 1):S66–S73.
38. Rolleman EJ, Forrer F, Bernard B, et al. Amifostine protects rat kidneys during peptide receptor radionuclide therapy with [^{177}Lu-DOTA^0,Tyr^3]octreotate. *Eur J Nucl Med Mol Imaging.* 2007;34:763–771.
39. Patrick TA, Kranz DM, vanDyke TA, Roy EJ. Folate receptors as potential therapeutic targets in choroid plexus tumors of SV40 transgenic mice. *J Neurooncol.* 1997;32:111–123.